Titanium Nano-Antenna for High-Power Pulsed Operation

Evgeny G. Mironov, Ziyuan Li, *Student Member, IEEE*, Haroldo T. Hattori, *Senior Member, IEEE*, Kaushal Vora, Hark Hoe Tan, *Senior Member, IEEE*, and Chennupati Jagadish, *Fellow, IEEE*

***Abstract*—While plasmonic nano-antennas can produce intense electric fields in a very small area, in general, these devices cannot handle high power, because of their small footprints. In order to increase the maximum peak power that these devices can withstand, they can be driven by nano-second pulses from a larger diameter Q-switched laser, which reduces the fluence reaching the devices, thus avoiding their destruction. Furthermore, we show that an increase in the power density capacity of the nano-antennas can be achieved by replacing gold with titanium: more than 18 dB greater power density can be handled by titanium based nano-antennas without significant reduction in their electric field enhancement capabilities.**

***Index Terms*—Nano-photonics, plasmonic nano-antennas, plasmonics, Q-switched laser.**

I. Introduction

THE advent of plasmonic nano-antennas has brought new light into the nano-world – whereby freely propagating optical radiation can be converted into localized optical fields and vice-versa [1]. These devices can confine light well below the diffraction limit [2], generating highly intense localized electric fields that can be used in a multitude of applications in nonlinear optics, imaging, sensing and photovoltaics [1].

The simplest nano-antenna device is a dipole antenna [2], [3], which is constructed by placing a dielectric gap between two metallic regions. In this structure, a strong electric field enhancement above 50 could be generated inside the dielectric gap when the device is excited by an external laser source. Besides dipole nano-antennas, more complex structures have also been studied such as Yagi-Uda [4], [5], spiral [6]–[8], phased-array [9] and staircase [10] nano-antennas, where they can either provide better directivity or operate at larger bandwidths when compared with dipole based counterparts.

Nano-antennas can be fabricated by using different equipment such as electron beam lithography (EBL), followed by lift-off techniques, focused ion beam milling (FIB) [10] and nano-stencil lithography [11]. In all these processes, gold is generally deposited on top of a thin layer of titanium [11]–[13], which provides better adhesion between the gold layer and the substrate. However, as mentioned by Lahiri and co-workers [13], the presence of the titanium layer changes the performance of the plasmonic devices with effects such as shifting of the resonant frequency of the devices. These effects are caused by different material properties such as larger absorption losses and different plasma frequencies [13].

Nano-antennas are passive devices that are excited by external light sources. Because of their small footprints, they cannot handle high power, where higher power leads to higher fluence (energy per unit area), which can eventually destroy the antennas. In general, metal ablation occurs first, destroying the metallic regions of the antenna. The incoming optical radiation is absorbed by the metal – leading to fast energy relaxation, thermal diffusion, and energy transfer to the lattice due to electron-phonon coupling [14], [15].

In order to increase the power capacity of nano-antennas and avoid metal ablation, different strategies can be used, such as: (1) increase of the spot-size of the optical source, (2) employment of pulsed sources and (3) judicious choice of the metallic materials. Strategies (1) and (2) lead to lower fluences per pulse and provide longer time for heat dissipation. A sensible choice of materials can produce devices that can handle larger fluences without melting and, at the same time, produce high electric field enhancement with good adhesion to the substrate (avoiding excessive mechanical stress to the nano-antenna). In this article, we analyze structures that are excited by an external large spot-size (the original spot diameter of 2 mm could be increased by an external optical lens) Q-switched laser (pulse duration of 10 ns with repetition rate of 5 kHz and operating at a wavelength of 1053 nm).

These devices are fabricated by using either gold or titanium. While gold is a common choice in plasmonic devices because of its relatively low losses, titanium is widely used in many applications ranging from aerospace and marine engineering to jewelery and medical implants. Also it is common practice to introduce a thin titanium adhesion layer prior to gold layer deposition on semiconductor and dielectric substrates [16], [17]. Our results show that titanium nano-antennas can handle considerably more power than their gold counterparts, without significantly reducing their electric field enhancement capacity.

II. Theoretical Analysis

Our nano-antenna consists of two metallic regions (orange areas) on top of a quartz substrate separated by an air gap as il-

Manuscript received September 07, 2012; revised February 14, 2013; accepted April 29, 2013. Date of publication May 02, 2013; date of current version June 24, 2013. This work was supported in part by the Australian Research Council (ARC) and in part by the Australian National Fabrication Facility (ANFF).

E. G. Mironov, Z. Li, and H. T. Hattori are with the School of Engineering and Information Technology, The University of New South Wales, Canberra ACT 2600, Australia (e-mail: Evgeny.Mironov@student.adfa.edu.au; Ziyuan.Li@student.adfa.edu.au; h.hattori@adfa.edu.au).

K. Vora, H. H. Tan, and C. Jagadish are with the Research School of Physics and Engineering, The Australian National University, Canberra ACT 0200, Australia (e-mail: kdv109@physics.anu.edu.au).

Color versions of one or more of the figures in this paper are available online at http://ieeexplore.ieee.org.

Digital Object Identifier 10.1109/JLT.2013.2261281

0733-8724/$31.00 © 2013 IEEE

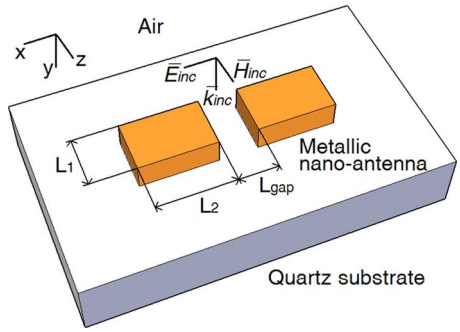

Fig. 1. Schematic of the nano-antenna structure.

lustrated in Fig. 1. Thus the device is a typical dipole antenna. The metallic material is either gold (with a very thin 2 nm titanium adhesion layer) or titanium.

In order to analyze the optical properties of the nano-antenna, commercial Finite Difference Time-Domain (FDTD) software is used [18]. The optical wave coming from the source is incident normally onto the nano-antenna, i.e., the propagation direction is assumed to be the y-direction. The electric field $\boldsymbol{E_{inc}}$ is oriented along the x-axis and directed across the air gap, as shown in Fig. 1. The computational region is terminated by perfectly matched absorbing borders. The grid is non-uniform, being refined at the boundaries between the metal and dielectric. The grid sizes for the dielectric and metallic regions are $\Delta x = \Delta y = \Delta z = 20$ nm and $\Delta x = \Delta y = \Delta z = 3$ nm, respectively. The grid size choice of 20 nm may be large for nano-antennas with small gaps, so we have checked the results with smaller grid sizes – $\Delta x = \Delta y = \Delta z = 5$ nm for the dielectric regions. However, there is less than 1% variation in the results. The step time is chosen as 8×10^{-18} s, which corresponds to less than half of the stabilization limit. (The very dispersive nature of the materials involved requires a very small time step to produce stable FDTD simulations).

Fullwave [18] uses the following dispersive model for metals:

$$\varepsilon\left(\omega_{Fullwave}\right) = 1 + \sum_{k}^{6} \frac{\Delta\varepsilon_k}{-a_k {\omega_{Fullwave}}^2 - b_k(i\omega_{Fullwave}) + c_k}, \quad (1)$$

where a, b, c and $\Delta\varepsilon$ are coefficients from the in-built materials library (see Table I below) and $\omega_{Fullwave}$ is the Fullwave computational frequency. It is important to note that Fullwave uses its own notation for frequency – and $\omega_{Fullwave}$ is normalized with respect to the speed of light [18] and therefore is expressed in $\mu\mathrm{m}^{-1}$:

$$\omega_{Fullwave} = \frac{\omega_0}{c_{vac}}, \quad (2)$$

where ω_0 is the angular frequency of the incoming radiation and c_{vac} is the speed of light in vacuum.

In the simulations, the incident wave is considered to be a plane wave, which is a good approximation because the actual spot-size diameter of the source is much larger than the computational area (this area is 10 μm by 10 μm, whilst the spot size of the source is several millimeters in diameter) and much larger than the dimensions of the device. After aligning the structure

TABLE I

Titanium				Gold			
Δε	a	b	c	Δε	a	b	ε
201.7403	1	0.41529	0	1589.516	1	0.268419	0
1225.436	1	11.52684	15.48524	50.19525	1	1.220548	4.417455
535.7023	1	12.75245	61.22558	20.91469	1	1.747258	17.66982
254.9016	1	8.42229	161.4646	148.4943	1	4.406129	226.0978
1.36311	1	8.923677	9683.258	1256.973	1	12.63	475.1387
0	0	0	0	9169	1	11.21284	4550.765

Dispersion coefficients from Fullwave material data base [18]

to the position of maximum peak power, the magnitude of the incident electric field $|\boldsymbol{E_{inc,peak}}|$ can be estimated as

$$|\mathbf{E_{inc,peak}}| \cong \sqrt{\frac{8 Z_{air} P_{peak}}{\pi \varphi_{spot}^2}}, \quad (3)$$

where Z_{air} is the intrinsic impedance of air ($\sim 377\ \Omega$), P_{peak} is the peak power of the wave (its value can be controlled by an attenuator), φ_{spot} is the spot size of the pulse (which can be expanded by passing the laser light through a divergent lens).

The nano-antennas have a metallization thickness of 300 nm and length $L_1 = 100$ nm. The structures are fabricated with air – gap widths L_{gap} ranging from 60 to 120 nm. The width of the metallic region L_2 (the nano-antenna arms have equal dimensions) is such that $2L_2 + L_{gap} = 425$ nm. The air gap is created by milling the metal with a focused ion beam (FIB) system. The space between the metallic regions will generate a higher electric field than the incident field, through the excitation of a plasmonic wave. The relationship between the magnitudes of the electric fields is the electric field enhancement factor, F_{gap}, which is given by

$$F_{gap} = \frac{|\mathbf{E}_{gap,peak}|}{|\mathbf{E}_{inc,peak}|}, \quad (4)$$

where $|\boldsymbol{E}_{gap,peak}|$ is the magnitude of the electric field measured in the middle of the nano-antenna gap. The magnitude of the electric field can be higher at the edges of the nano-antenna (i.e the interface between the metal and the air gap): for example, for a gold nano-antenna with a gap width of 60 nm, F_{gap} is 4.39, whilst the electric field enhancement can reach 7.3 at the edges of the nano-antenna. However, the higher electric field enhancements at the edges of the nano-antenna will be reduced during the fabrication process because of fabrication imperfection, which makes the edges smoother and not abrupt. From FDTD calculations, the electric field enhancement factor as a function of the gap width is plotted in Fig. 2, at a wavelength of 1053 nm. This factor changes very little with the spot-size of the source, given that it is much larger than the area of the nano-antennas.

In Fig. 2, the field enhancement factor for gold is about 18% higher than for titanium, mainly because the latter has larger losses. The values of F_{gap} for both materials are presented in Table II.

To have a more precise comparison for each gap width, the total length of the nano-antenna should be optimized to produce the highest electric field enhancement. This optimization

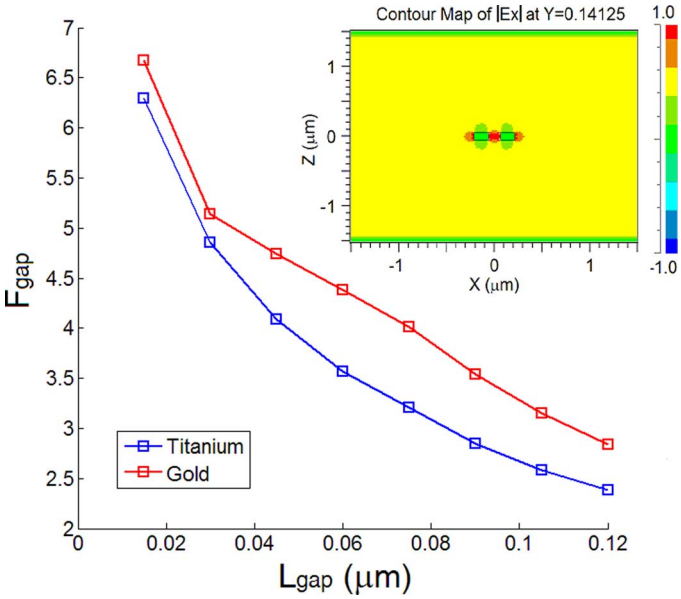

Fig. 2. Electric field enhancement factor F_{gap} as a function of the gap width L_{gap}. Inset – field profile for a $L_{gap} = 120$ nm.

TABLE II

L_{gap}, nm	F_{gap} (gold)	F_{gap}(titanium)
120	2.84	2.39
105	3.15	2.59
90	3.54	2.85
75	4.01	3.21
60	4.39	3.56
45	4.74	4.09
30	5.14	4.86
15	6.67	6.29

Electric field enhancement factor F_{gap} as a function of the gap width L_{gap}

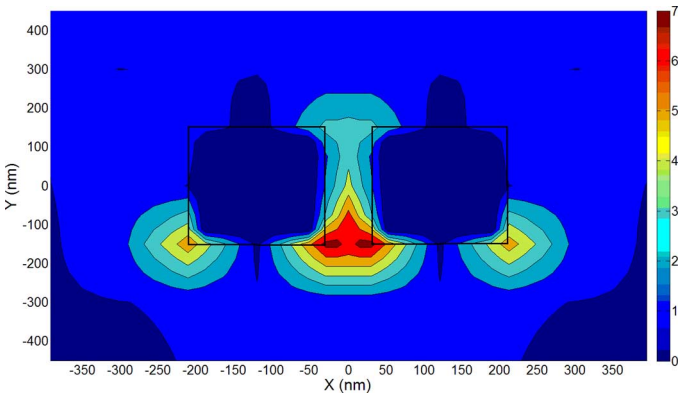

Fig. 3. Electric field strength (x-y plane) for gold nano-antenna.

process (for gold and titanium) is conducted for two gap widths – 60 and 120 nm – and the change in the field enhancement is less than 6%. Hence, in our case, we have only varied the width of the air gap in our experiments, while keeping the total length of the nano-antenna constant.

The plots of the electric field distribution in the gold and titanium nano-antennas are shown in Figs. 3–6. Figs. 3 and 5 show the field distribution along the x-y plane containing the nano-antenna ($z = 0$ nm, slice taken in the middle of the gap), while

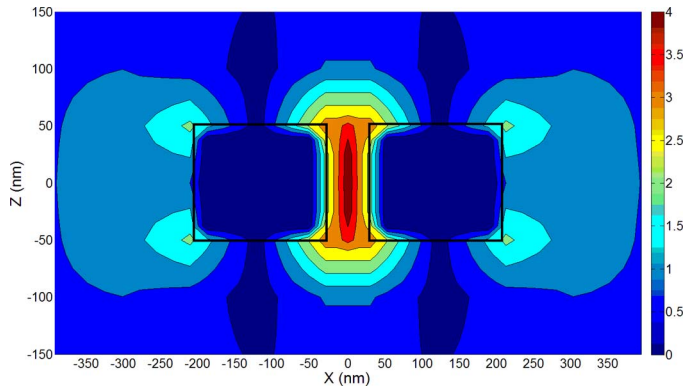

Fig. 4. Electric field strength (x-z plane) for gold nano-antenna.

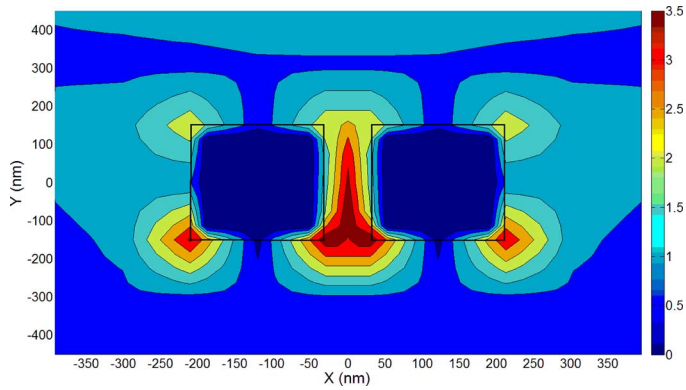

Fig. 5. Electric field strength (x-y plane) for titanium nano-antenna.

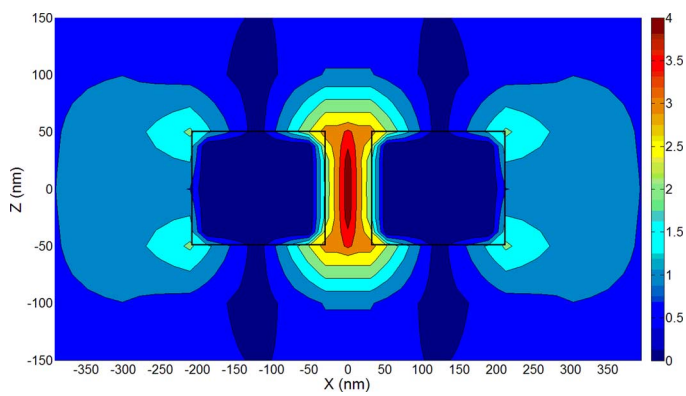

Fig. 6. Electric field strength (x-z plane) for titanium nano-antenna.

Figs. 4 and 6 show the field distribution along the x-z plane containing the nano-antenna ($y = 150$ nm, slice taken at the half-height of the nano-antenna metallization) for gold and titanium, respectively. The gap width is assumed to be 60 nm, but similar results are obtained for different gap widths. An extensive number of electric field monitors (more than 75) is placed in the region close to the nano-antenna to measure the distribution of the magnitudes of electric field $|\boldsymbol{E_y}|$. It can be observed that the electric field is higher at the edges of the nano-antenna that are close to the air gap – but over a very limited region. More importantly, the electric field distribution is more uniform in the titanium nano-antenna, providing a lower power density when compared to the gold antenna. This result can partially

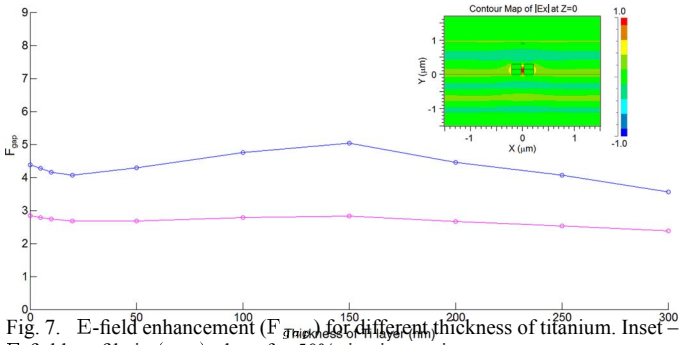

Fig. 7. E-field enhancement (F_{gap}) for different thickness of titanium. Inset – E-field profile in (x, y) plane for 50% titanium ratio.

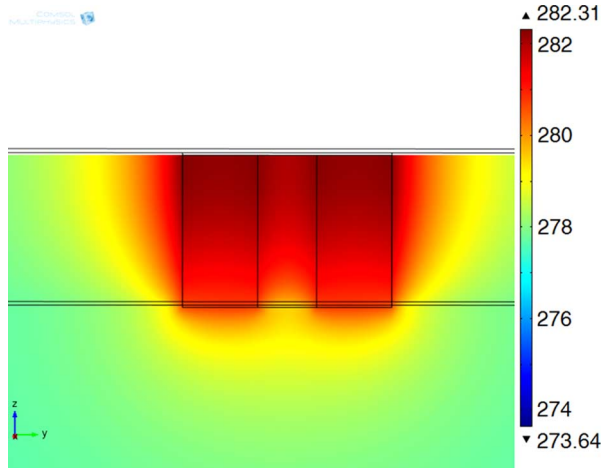

Fig. 8. Qualitative temperature distribution in a titanium nano-antenna. Temperature is given in °C.

explain the fact that titanium based nano-antennas can handle more power than their gold counterparts.

In our experimental section, a 2 nm thick titanium layer is deposited as the adhesion layer, prior to gold deposition. In order to study the impact of this titanium layer on the electric field enhancement of the nano-antenna, the thickness of the titanium/gold bilayer is varied from 0 to 300 nm, with the total height fixed at 300 nm. The results are presented in Fig. 7 for 120 nm (magenta) and 60 nm (blue) gap widths. The maximum value of F_{gap} is reached when the thickness of titanium in the nano-antenna reaches 50% – an increase in F_{gap} of about 15% over the value for gold is produced, which can be partially explained by the stronger field localization close to the interface between the gold and the titanium, as shown in the inset of Fig. 7.

The electric field enhancement provided by the nano-antenna can be used in a variety of applications such as nano-imaging, detection of nano-particles, sensing and nonlinear effects. For example, in the surface enhanced Raman scattering (SERS) effect, the enhancement factor is proportional to the fourth power, i.e., to F_{gap}^4, meaning that huge enhancements can be obtained by using nano-antennas [10].

The physical parameter that is generally associated with the damage of a material is the fluence [15]. In the case of a Q-switched laser, the energy of a single pulse, $W_{single\text{-}pulse}$ and the fluence $F_{single\text{-}pulse}$, are given by,

$$W_{single-pulse} = \int_{t_1}^{t_2} P(t)dt = P_{peak}\tau_{eff} \qquad (5.1)$$

$$F_{single-pulse} = W_{single-pulse}\frac{4}{\pi\varphi_{spot}^2}, \qquad (5.2)$$

where $P(t)$ is the envelope of the power as a function of time, t_1 and t_2 are arbitrary instants when the pulse power is not negligible ($t_1 < t < t_2$) and τ_{eff} is the effective duration of the pulse. In a given exposure interval, T_{ref} and repetition rate, f_{rep}, the number of pulses in that time period, N_{pulse} is $N_{pulse} = T_{ref} \cdot f_{rep}$. Then the exposure F_{ex} and effective F_{eff} fluences are given by,

$$F_{ex} = N_{pulse}W_{single-pulse}\frac{4}{\pi\varphi_{spot}^2} \qquad (6.1)$$

$$F_{eff} = N_{pulse}^{p}W_{single-pulse}\frac{4}{\pi\varphi_{spot}^2}. \qquad (6.2)$$

The calculation of the effective pulse energy in a given exposure time interval follows the calculations for laser safety in the Australian/New Zealand laser safety standards [19]. The parameter, p is a variable with values between 0 and 1. It takes into account the fact that the structures can cool in the interval between two consecutive pulses. If during this time the structures cool, then $p = 0$ and the effect of each pulse on the nano-antennas will be independent. On the other hand, if thermal effects are very slow, then the exposure to successive pulses will have a cumulative effect and $p = 1$. As an example of an intermediate situation ($0 < p < 1$), we cite the case of the human eye, for which $p = 0.25$ [19] at low repetition rates (f_{rep} below 10 kHz).

Both Chang and co-authors [20] and Link and co-authors [21] have studied the melting of gold nano-particles using nano-second [20] and femto-second [21] lasers. Chang [20] has observed that different laser fluences can lead to different phase transitions and shapes of nano-rods. In another experiment, Link [21] observed that it takes tens of pico-seconds for nanorods to melt, which seems to imply that the small volume of the nano-particles results in rapid heating and cooling effects. In the case of nano-second lasers, the longer pulse duration leads to cumulative heating effects [20] but the nano-antennas may cool down more quickly because of their small footprint, suggesting the independence of each pulse in the heating of these structures ($p = 0$). However, it should be mentioned that it will take a much longer time for the substrate to cool because of its considerably larger volume.

It is hard to model fully the heating of plasmonic nano-antennas. For nano-second pulses, the duration of each pulse is significantly longer than the lattice heating time and thus thermalization between the electron subsystem and the lattice takes place [14] and the system can be analyzed by solving the heat diffusion equation.

The temperature distribution of the structure when it is illuminated by laser radiation is analyzed by solving the heat equation with COMSOL software [22]. There are two main mechanisms that can cause thermal damage, which are direct laser heating of the exposed material and heating due to enhanced localized electric field (plasmonic heating) that arises in the nano-antenna gap region. Fig. 8 shows the qualitative temperature distribution inside the structure when the laser light reaches the surface. It is clear that the metallic and air gap regions have a higher temperature that of than the surrounding air and the quartz substrate.

TABLE III

Material	Volumetric heat capacity, $J \cdot cm^{-3} \cdot K^{-1}$	Thermal conductivity, $W \cdot m^{-1} \cdot K^{-1}$
Gold	2.492	318
Air	0.00121	0.0257
Titanium	2.359	22
Quartz	1.661	1.3

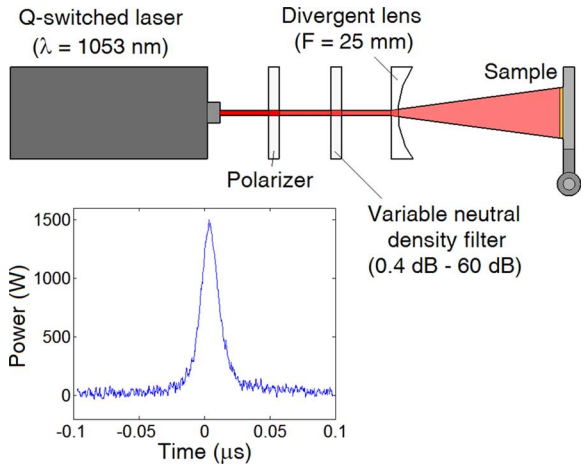

Fig. 9. Experimental setup. Inset – single pulse profile.

The heat coefficients for the materials are summarized in Table III. These data indicate that the heat generated by nano-antennas is not efficiently dissipated by the surrounding air and the quartz substrate, leading to a hot spot in the metallic areas. As shown in Fig. 8, heat concentrates in the nano-antenna region and heat therefore cannot easily diffuse into the surrounding region.

III. Experimental Results

The experimental setup is presented in Fig. 9. A commercial Q-switched laser, operating at 1053 nm, with single pulse energy of 15 μJ has been used in the experiments (the single pulse profile is shown in the inset in Fig. 9). The duration of each pulse is 10 ns, the total exposure time is 300 s and a repetition rate of 5 kHz is typically used. In some experiments, the repetition rate is varied from 2 to 10 kHz and the exposure time from 300 to 1000 s. No significant change in the results is found from this study. A variable metallic-film neutral density filter that allows the alteration of the attenuation from 0.4 to 60 dB is used to control the incident fluence. The original spot-size of the laser beam φ_{spot} is 2 mm in diameter, but it can be expanded to larger values by using a divergent lens with a focal length of 25 mm. With this setup we have the ability to change the laser fluence over a wide range (by more than 80 dB). Finally, to ensure that the main electric field is along the x-axis, as in Fig. 1, a polarizer is placed between the Q-switched laser and the lens.

As mentioned previously, the thickness of the metal (gold or titanium) is 300 nm and the materials are deposited using an electron beam evaporator. In the case of the gold nano-antennas, a 2 nm thick layer of titanium is added on top of quartz prior to gold deposition to improve adhesion. After the deposition of the metallic layers, the structures are milled using an FEI Helios NanoLab 600 dual-beam FIB system. The area occupied by the patterns is about 100 μm by 100 μm, while the remaining part is covered with metal. The whole sample area is 1 cm by 1 cm. The refractive indices of gold and titanium at 1053 nm are $\mathrm{n_{gold}} = 0.23 - \mathrm{j} \cdot 7.10$ and $\mathrm{n_{titanium}} = 3.453 - \mathrm{j} \cdot 4.004$ respectively. These values for the complex refractive indices mean that, when gold (titanium) is used, about 98% (62%) of the incident power is reflected back towards the laser and attenuator system.

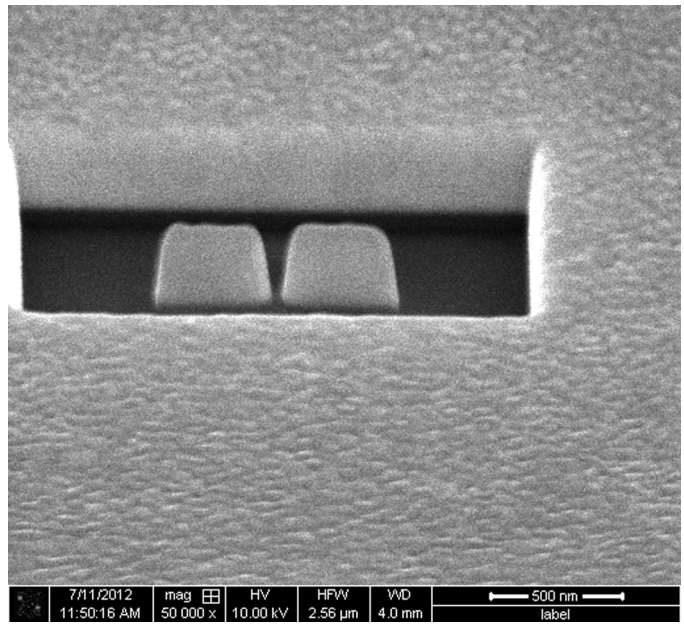

Fig. 10. SEM image of a 60 nm gap gold nano-antenna.

Fig. 10 shows a scanning electron microscope (SEM) image of a nano-antenna after fabrication. It can be seen that the walls are not perfectly vertical and the gap width at the mid-height of the gold region is about 60 nm. Structures with a gap width of 120 nm have also been fabricated and have almost vertical walls.

After exposure to laser light at a given fluence, another SEM image was taken to assess the potential damage to the nano-antennas (Fig. 11). The experiments were primarily focused on two samples with gap widths of 60 nm and 120 nm. The damage fluence threshold was measured mainly for the 60 nm gap nano-antenna. For gold nano-antennas, the single pulse damage fluence was $F_{single\text{-}pulse} = 0.059\,\mathrm{J/m^2}$ and the total exposure fluence ($T_{ref} = 300\,\mathrm{s}$ and $f_{rep} = 5\,\mathrm{kHz}$) was $F_{ex} = 88.5\,\mathrm{kJ/m^2}$. Note that the main damage to the nano-antenna occurs in its central gap region, where there is a high value of field enhancement.

In fact, the melting of the metal regions filled this space with gold. The 120 nm gap nano-antennas melts at a higher fluence, but it is hard to determine the threshold fluence because of the discrete attenuation steps of the variable metallic-film neutral density filter (by about less than double the fluence of the 60 nm gap).

For the titanium nano-antennas shown in Fig. 12, the walls are not perfectly vertical either. The gap width at the mid-height of the nano-antenna is 60 nm. For other structures, which have wider gaps, the walls become more vertical, as well.

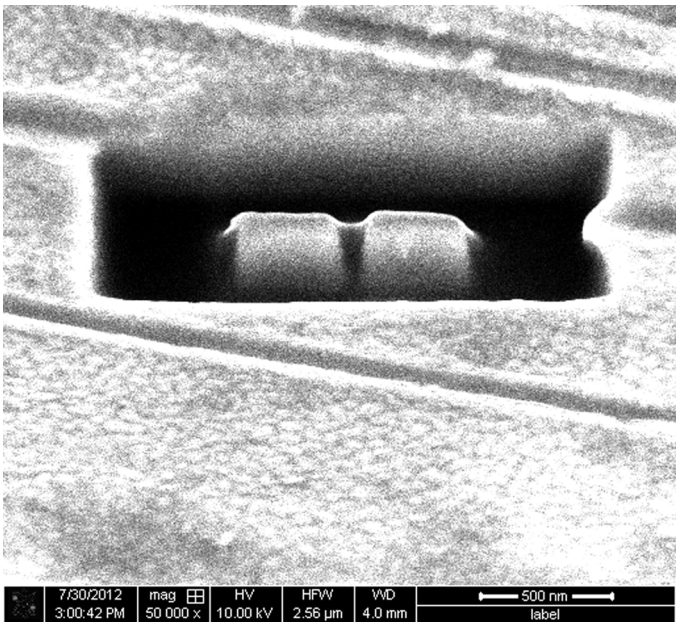

Fig. 11. SEM image of a 60 nm gap gold nano-antenna with clear melting of the gold regions.

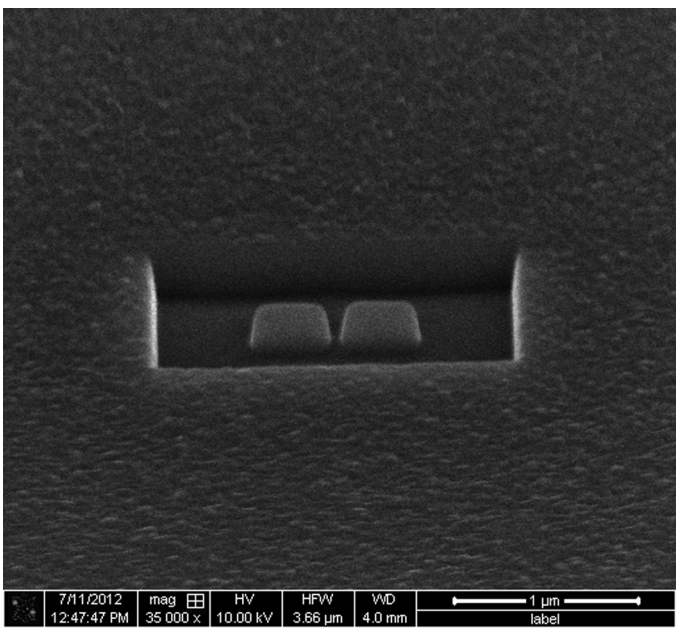

Fig. 12. SEM image of a 60 nm gap titanium nano-antenna.

After exposing the 60 nm gap titanium structure to laser light during a period of 5 minutes, the damage single pulse fluence was estimated to be 4.35 $\mathrm{J/m^2}$, whilst the total exposure fluence was 6525 $\mathrm{kJ/m^2}$.

An SEM image of the damaged titanium nano-antenna is shown in Fig. 13. In comparison with its gold counterpart, the damage threshold fluence has increased by a factor of 74, although the electric field enhancement is reduced by 19% (for a 60 nm gap, with the data presented in Table I). Thus titanium based structures could withstand and create about 7 times higher electric fields than gold nano-antennas and are considerably more power resistant.

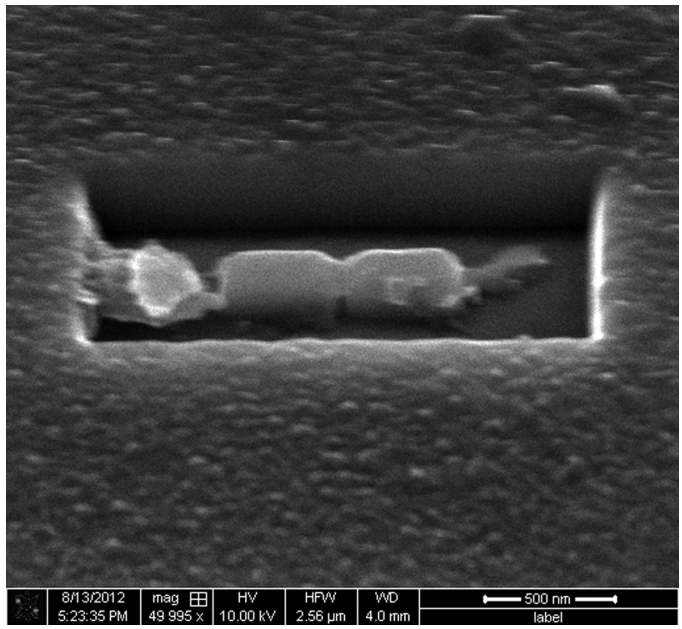

Fig. 13. SEM image of a 60 nm gap titanium nano-antenna with clear melting of the titanium regions.

Possible explanations for the better performance of titanium devices over their gold counterparts include: (1) higher melting temperature (1668°C against 1064°C), (2) larger mechanical strength, and (3) increased penetration depth, which means that the fields will permeate deeper into metal and the power density will be less localized on the surface of titanium nano-antennas. Lahiri and co-workers [13] have analyzed the effect of titanium on split-ring resonators and attributed the shift in the resonant frequency of the meta-material as being due to the difference in the skin depth of the metals.

IV. Conclusion

In this article, high power pulsed nano-antennas have been analyzed. These structures are excited by nano-second pulses coming from a large spot-size Q-switched laser. It is shown that titanium based devices produce 19% lower electric field enhancement than gold nano-antennas but they can withstand about 74 times higher fluence and, consequently, are capable of producing 7 times higher magnitude of electric fields than gold nano-antennas. Potential applications to surface enhanced Raman scattering (SERS), nano-imaging, nano-particle detection, nonlinear optics, and other high power applications can be envisioned with titanium based nano-antennas.

References

[1] P. Bharadwaj, B. Deutsch, and L. Novotny, "Optical antennas," *Adv. Opt. Photon.*, vol. 1, pp. 438–483, 2009.

[2] N. Yu, E. Cubukcu, L. Diehl, D. Bour, S. Corzine, J. Zhu, G. Höfler, K. B. Crozier, and F. Capasso, "Bowtie plasmonic quantum cascade laser antenna," *Opt. Exp.*, vol. 15, pp. 13272–13281, 2007.

[3] H. T. Hattori, Z. Li, D. Liu, I. D. Rukhlenko, and M. Premaratne, "Coupling of light from microdisk lasers into plasmonic nano-antennas," *Opt. Exp.*, vol. 17, pp. 20878–20884, 2009.
[4] T. Kosako, Y. Kadoya, and H. F. Hofmann, "Directional control of light by a nano-optical Yagi-Uda antenna," *Nature Photon.*, vol. 4, pp. 312–315, 2010.
[5] T. H. Taminiau, F. D. Stefani, and N. F. van Hulst, "Enhanced directional excitation and emission of single emitters by a nano-optical Yagi-Uda antenna," *Opt. Exp.*, vol. 16, pp. 10858–10866, 2008.
[6] C. Fumeaux, G. Boreman, W. Herrmann, H. Rothuizen, and F. Kneubühl, "Polarization response of asymmetric-spiral infrared antennas," *Appl. Opt.*, vol. 36, pp. 6485–6490, 1997.
[7] J. Alda, J. Rico-García, J. López-Alonso, and G. Boreman, "Optical antennas for nano-photonic applications," *Nanotechnology*, vol. 16, pp. S230–S234, 2005.
[8] F. González and G. Boreman, "Comparison of dipole, bowtie, spiral and log-period IR antennas," *Infrared Phys. Technol.*, vol. 146, pp. 418–428, 2004.
[9] C. Middlebrook, P. Krenz, B. Lail, and G. Boreman, "Infrared phased-array antenna," *Microw. Opt. Technol. Lett.*, vol. 50, pp. 719–723, 2008.
[10] Z. Li, H. T. Hattori, P. Parkinson, J. Tian, L. Fu, H. H. Tan, and C. Jagadish, "A plasmonic staircase nano-antenna device with strong electric field enhancement for surface enhanced Raman scattering (SERS) applications," *J. Phys. D: Appl. Phys.*, vol. 45, no. 305102, pp. 1–5, 2012.
[11] S. Aksu, A. A. Yanik, R. Adato, A. Artar, M. Huang, and H. Altug, "High-throughput nanofabrication of infrared plasmonic nanoantenna arrays for vibrational nanospectroscopy," *Nano Lett.*, vol. 10, pp. 2511–2518, 2010.
[12] A. Kinkhabwala, Z. Yu, S. Fan, Y. Avlasevich, K. Müllen, and W. E. Moerner, "Large single-molecule fluorescence enhancements produced by a bowtie nanoantenna," *Nature Photon.*, vol. 3, pp. 654–657, 2010.
[13] B. Lahiri, R. Dylewicz, R. M. De La Rue, and N. P. Johnson, "Impact of titanium adhesion layers on the response of metallic split-ring resonators (SRRs)," *Opt. Exp.*, vol. 18, pp. 11202–11208, 2010.
[14] M. E. Fermann, A. Galvanauskas, and G. Sucha, *Ultrafast Lasers: Technology and Applications*. New York, NY, USA: Marcel Dekker, 2003, pp. 359–394.
[15] H. Sobral and M. Villagrán-Muniz, "Energy balance in laser ablation of metal targets," *J. of Appl. Phys.*, vol. 98, pp. 083305 1–5-, 2005.
[16] B. Kante, J.-M. Lourtioz, and A. de Lustrac, "Infrared metafilms on a dielectric substrate," *Phys. Rev. B*, vol. 80, p. 205120, 2009.
[17] F. Gadot, B. Belier, A. Aassime, J. Mangeney, A. de Lustrac, and J.-M. Lourtioz, "Infrared response of a metamaterial made of gold wires and split ring resonators deposited on silicon," *Opt. Quantum Electron.*, vol. 39, no. 4–6, 2007.
[18] *Fullwave 6.0 RSOFT Design Group*, , 1999 [Online]. Available: http://www.rsoftdesign.com
[19] *Australian/New Zealand Standard AS/NZS 2211.1*, 2004- Safety of Laser Products.
[20] S. S. Chang, C. W. Shih, C. D. Chen, W. C. Lai, and C. R. C. Wang, "The shape transition of gold nanorods," *Langmuir*, vol. 15, pp. 701–709, 1999.
[21] S. Link, C. Burda, B. Nikoobakht, and M. A. El-Sayed, "How long does it take to melt a gold nanorod? A femtosecond pump-probe absorption spectroscopy study," *Chem. Phys. Lett.*, vol. 315, pp. 12–18, 1999.
[22] COMSOL 4.0 Multiphysics 2012 [Online]. Available: http://www.comsol.com

Evgeny G. Mironov graduated from the Moscow Institute of Physics and Technology with Bachelor (2008) and Masters (2010) degrees in Applied Mathematics and Physics. During his studies, he had a part-time job as a Senior Lab Assistant at the Institute for High Pressure Physics (Russian Academy of Sciences). Since July 2011 he has been a PhD student at UNSW (Canberra) and visiting student at the Australian National University. His main interests are in meta-materials, plasmonics and lasers.

Ziyuan Li was born in 1987 in China and received her Bachelor of Engineering degree from Beijing Institute of Technology in 2009 with a major in Optical and Electronics Engineering. She is a Ph.D graduate from the School of Engineering and Information Technology, UNSW and was also a visiting student at the Australian National University, where she worked in collaboration with Prof. Jagadish. Her work focuses on various topics, including both the design and fabrication of lasers and photodetectors coupled to plasmonic devices.

Haroldo T. Hattori (M'00–SM'08) received his B.Sc. (with honors) and M.Sc. degrees from Instituto Tecnológico de Aeronáutica (ITA), Brazil and his PhD degree from Virginia Polytechnic Institute and State University in 1998. All degrees are in Electrical Engineering.

He worked as an optical fiber communications engineer for Alcatel (1989–1994) in Brazil and Spain. In 1994, he left Alcatel to work towards his PhD degree at Virginia Tech. His thesis analyzed the detrimental effects of nonlinearities and dispersion in very long-distance optical fiber links. In 1998, he returned to Brazil where he became an Assistant Professor at ITA and worked on the development of fiber Bragg gratings sensors and communication devices. From 2002 to 2005, he worked as a post-doctoral researcher at the University of Glasgow (Glasgow UK) and Ecole Centrale de Lyon (Lyon France) on integrated optical components (photonic crystal passive and active devices and microdisk lasers).

In 2006, he moved to Australia where he is currently a Senior Lecturer at the School of Engineering and Information Technology, the University of New South Wales at Canberra. He is also a visiting Fellow at the Australian National University. His main interests include semiconductor-based integrated optics (mostly active devices), plasmonics, meta-materials, optical fibers and nanotechnology.

Dr. Hattori is a Senior Member of the Institute of Electrical and Electronic Engineers (IEEE), a Senior Member of the Optical Society of America (OSA), a Member of Engineers Australia, a Member of the Phi Kappa Phi and Eta Kappa Nu Honor Societies.

Kaushal Vora received his BE in Electrical Engineering in 1996 from Saurashtra University, India. He moved to Australia and obtained a Masters degree in Microsystems Technology in 2004 from Swinburne University of Technology, Australia. His master's thesis was focused on integrating microfludic channel with an optical waveguide to create a low-cost biosensor. He acquired PhD degree in 2009 from La Trobe University, Australia during which he developed processes to fabricate densely-packed high aspect-ratio microstructures using x-ray lithography. He worked as a Research Officer at La Trobe University, where, he was involved in design, fabrication and testing of x-ray optics for phase-contrast imaging using μ-XCT. He joined The Australian National University in 2009 as a process engineer for ANFF ACT node. His research include micro/nano fabrication of silicon and III-V based devices, thin-film deposition and patterning of metal and insulator layers, optical waveguides, solar-cell devices, p-silicon nanowire growth and nano-replication techniques.

Hark Hoe Tan (SM'03) received his B.E. (Elec.) and PhD degrees from the University of Melbourne and the Australian National University, in 1992 and 1997, respectively. In 1992, he joined Siemens Opto-Semiconductor, Penang, where he worked in the area of quality assurance. His doctoral dissertation was on ion beam effects in GaAs-AlGaAs materials and devices. He was a former recipient of the prestigious Australian Research Council Queen Elizabeth II fellowship. Dr. Tan's research area covers both the fundamental and applied aspects of compound semiconductors and he has published over 180 journal papers. The two main contributions of his work to the field are in the MOCVD growth of nanostructures and the ion implantation of semiconductors for optoelectronic applications. He is currently a Senior Fellow at the Australian National University.

Chennupati Jagadish (S'84–M'86–SM'92–F'02) was born and educated in India (BSc, Nagarjuna, MSc(Tech), Andhra, MPhil, PhD, Delhi) and worked in India (S.V. College, New Delhi) and Canada (Queen's University, Kingston, Ont), prior to moving to Australia in 1990. He is currently an Australian Laureate Fellow, Distinguished Professor and Head of Semiconductor Optoelectronics and Nanotechnology Group in the Research School of Physics and Engineering, Australian National University. He is also Convenor of the Australian Nanotechnology Network (more than 1500 members) and Director of Australian National Fabrication Facility, ACT Node. He served as President of the IEEE Nanotechnology Council (NTC) during 2008, 2009 and Vice-President (Membership and Region Affairs – Asia Pacific) of IEEE Lasers and Electro-Optics Society during 2006, 2007 and currently serving as Vice-President (Finance and Administration) of IEEE Photonics Society and Vice-President and Secretary, Physical Sciences of the Australian Academy of Science. Prof. Jagadish is an Editor of IEEE Electron Device Letters, Progress in Quantum Electronics, Journal of Semiconductor Technology and Science, Associate Editor of Journal of Physics D: Applied Physics and Beilstein Journal of Nanotechnology and serves on editorial boards of 12 other journals. He advises many high tech companies in Australia and overseas and collaborated with scientists from 20 countries. His research interests include quantum dots, nanowires, quantum dot solar cells, nanowire solar cells, quantum dot lasers, quantum dot photodetectors, quantum dot photonic integrated circuits, photonic crystals, plasmonics, metamaterials, THz photonics. He has published more than 700 research papers (470 journal papers), holds 5 US patents, co-authored a book, co-edited four books and edited 12 conference proceedings and 11 special issues of journals. He won the 2000 IEEE Millennium Medal and received Distinguished Lecturer awards from IEEE Nanotechnology Council, IEEE Photonics Society and IEEE Electron Devices Society. He is a Fellow of the Australian Academy of Science, Australian Academy of Technological Sciences and Engineering, IEEE, American Physical Society, Materials Research Society, Optical Society of America, American Vacuum Society, Electrochemical Society, SPIE-the International Society for Optical Engineering, American Association for Advancement of Science, Institute of Physics (UK), Institution of Engineering and Technology (UK), the Institute of Nanotechnology (UK) and the Australian Institute of Physics. He received Australian Federation Fellowship in 2004 and Australian Laureate Fellowship in 2009 from the Australian Research Council and Peter Baume Award from the ANU in 2006, the Quantum Device Award from International Symposium on Compound Semiconductors in 2010, IEEE Photonics Society Distinguished Service Award in 2010, ANU Top Supervisor Award in 2010, IEEE Nanotechnology Council Distinguished Service Award in 2011 and Electronics and Photonics Division Award of the Electrochemical Society in 2012.